Detecting Risk and Anomalies in Airplane Dynamics Through Entropic Analysis of Time Series Data

Ezequiel Juarez Garcia*
University of Florida, Gainesville, FL, 32611

Chad L. Stephens†
NASA Langley Research Center, Hampton, VA 23681

Nicholas J. Napoli‡
University of Florida, Gainesville, FL, 32611

Despite recent efforts to move away from traditional threshold exceedance detection methods for aircraft state monitoring, modern aircraft still rely on safety thresholds to communicate to pilots the identification of an anomaly in the aircraft when a threshold is surpassed. Current anomaly detection methods mainly depend on uninterpretable machine learning models to learn complex patterns and relationships contained in the time series data of aircraft. Although these methods are capable of identifying known anomalies, their deficiency in interpretability presents a challenge when translating them to different aircraft. To overcome this deficiency, entropic analysis of aircraft dynamics seeks to characterize the complexity, or lack thereof, of the aircraft dynamics prior to the development of a risk scenario. This complexity characterization provides a more straightforward summary of state changes in the dynamics of flight variables. To build a foundation for entropic analysis, we analyzed the complexity of unstable approaches, an anomalous event present in many of today's aviation accidents. The analysis revealed a statistically significant difference in the complexity distribution of flight variables under a stable approach versus an unstable approach. These differences in complexity were especially notable minutes before an approach was identified as unstable. Moreover, the multiscale entropic analysis revealed the presence of signal complexity at multiple time scales across multiple time windows before landing. By capturing state changes and corrections in the aircraft dynamics using entropy, advanced, yet still interpretable, sensor systems based on entropic frameworks from this study can be constructed in the future using classical machine learning approaches.

I. Introduction

Aviation incidents and accidents are less prevalent but airlines and federal aviation agencies continue to examine aviation data to reduce risk and further improve aviation safety. As such, agencies like the Federal Aviation Administration (FAA), National Transportation Safety Board (NTSB), and National Aeronautics and Space Administration (NASA) recognize the importance of aviation safety by regularly publishing advisories [1], accident reports [2], and strategic plans and concept of operations documents [3, 4]. However, despite current safety guidelines, protocols, and measures, and the general downward trend in civil aviation accidents over the last decade, the national airspace system (NAS) will need to adapt to the introduction of new aviation systems and factors that have the potential to disrupt the status quo of operational safety. For instance, with the projected doubling of air traffic [5] due to factors such as the growing number of unmanned autonomous systems (UAS) [6] and the rise in passenger load factor [7], new informed and proactive safety measures are being increasingly pursued by agencies. These measures need to be designed to identify and mitigate anomalies ahead of time to reduce the likelihood of an accident. This will require the study of different approaches for identifying risk and anomalies in flight dynamics, especially those that yield insight on and can be translated to future autonomous aviation systems.

The push for safety algorithms that are directly applicable to aircraft in the future national airspace is driven by safety initiatives and projects funded by federal agencies that not only seek to continue driving the safety factor of

---

*Graduate Research Assistant and L3Harris Fellow in the Human Informatics and Predictive Performance Optimization (HIPPO) Laboratory, Department of Electrical and Computer Engineering, AIAA Student Member (e-mail: ejuarezgarcia@ufl.edu).

†Researcher, Crew Systems & Aviation Operations Branch (e-mail: chad.l.stephens@nasa.gov).

‡Assistant Professor and Director of the Human Informatics and Predictive Performance Optimization (HIPPO) Laboratory, Department of Electrical and Computer Engineering, AIAA Senior Member (e-mail: n.napoli@ufl.edu).

aviation below target thresholds, but also to gain insight into how current approaches for identifying and mitigating flight risk can translate to future flight operations. The future airspace is expected to integrate aircraft with varying degrees of control and decision autonomy [4, 8]. The varying aeronautical requirements of these aircraft, such as airframe design and degree of human control and intervention, will demand a synergistic relationship between autonomous systems and human operators in order for them to operate safely within the same environment. Consequently, current safety programs are placing an increasing emphasis on developing interpretable and generalizable risk detection algorithms. One key project pursuing these goals is NASA's System-Wide Safety (SWS) project [9]. SWS objectives include: 1) examine aviation flight data linked to risk and 2) translate insights and algorithms obtained from current flight data to autonomous systems and study links to risk. These objectives highlight the need for new and informed algorithms capable of running on different aviation systems with minimal to no redesign required in the translation process. The realization of these objectives will speed up the development of other programs aimed at improving not only safety in aircraft but the overall safety of the national airspace system.

Currently, flight operation quality assurance methods predominately utilize univariate exceedance thresholds for various safety performance metrics recorded by flight data recorders (FDRs) [10, 11]; thus, when flights do not conform to the established exceedance threshold, that flight parameter is considered out of safety bounds. Regarding cybersecurity, complex malicious response injection attacks (CMRI) and other intrusions are designed with the perpetrator having working knowledge of the control system and covertly introducing malicious perturbations within the system's normal operating boundaries (e.g. statistical upper and lower bounds of the system) [12–14]. Furthermore, these statistical based detection methods are still utilized today for defining cyber-attacks for UAV operations [14]. Aircraft system condition monitoring provides real time insight into an aircraft's performance by quickly identifying unforeseen system failures and anomalies [15, 16]. During this analysis, systems predominately utilize threshold based measures or machine learning (ML) motivated models to classify system data as 'healthy' or 'anomalous' [11]. Early anomaly identification from data monitoring results in quicker maintenance response time and mitigates both unidentified and/or catastrophic system failure, thereby reducing human loss or injury and extending aircraft life-cycles [15–17].

It is evident that the majority of aviation systems use classical exceedance detection algorithms (EDA) which depend on a designed set of "rules," thus becoming limited to only detecting failure/failure patterns that are known to exist [12, 18, 19]. EDA has many methodological approaches, some are threshold-based and others mimic statistical process controls methodologies, which cannot capture complex interactions at a multivariate level [17, 20]. More advanced machine learning methods have been applied to examine multivariate parameters that describe aviation safety, flight dynamics, and system health [21–23]. These ML methods rarely explore or simply do not utilize any type of feature engineering approaches from a uni-variate or multivariate viewpoint. We directly rely on the ML algorithm to uncover the embedded temporal information and their multivariate interactions [23]. Thus, the ML approaches for such sequential flight data requires temporal models for improved accuracy [22]. This sometimes requires additional information about the analyzing data streams in order to effectively analyze the system, such as the expected number of change points and varying system states [24]. To overcome these problems, novel machine learning methods specifically target anomalies for specific applications (e.g., a specific anomaly related to a specific risk or related to a specific airplane design). However, these advanced ML approaches may not build upon furthering the fundamentals of developing a more generalized approach that captures complex variable dynamics across different risk profiles and aeronautical design. Thus, the translation from one aeronautical design to another design (e.g., A320 to 747 to Bombardier), maybe not translatable under one ML model. These ML methods utilize supervised learning methods that require large annotated data sets for specific cases [17, 20, 25]. Therefore, ML approaches are limited to only detecting "known system dynamics", where the ML output and model may still not be interpretable to the user. Thus, such models may not be translatable later to fully understanding the ideal flight dynamics for autonomous flight systems.

The development of generalized feature engineering approaches within the multivariate time series may provide a better translation for capturing the risk associated to future autonomous flight systems. Such proposed featuring engineering methodologies that characterized temporal changes can be translated and compared across multiple aeronautical designs. In addition, the application of such signal processing methods that already have the temporal information embedded in the feature can then be translated to more simplistic interpretable classical ML model (in which the ML algorithm itself doesn't factor in sequential data). Our main goal is to develop and evaluate an interpretable time series analysis method that is sensitive to system states change dynamics for use with various detection paradigms (ML frameworks), where classical statistical methods fail to provide the necessary discrimination across multiple aeronautical designs.

Entropic analysis aims to characterize a system based on its complexity, or lack thereof, by quantifying similarity and structure within the signal with distances metrics, rank order measures, or correlations[26, 27]. Currently, novel

2

entropic methods have been utilized to overcome these classical exceedance methods [28], by quantifying the complexity (inversely thought of as the predictability) of the signal. Thus, these entropic methods that quantify complexity of a time series signal can have the same statistical distribution but different complexities. To establish the validity of using entropic methods on the flight dynamics of aircraft, we investigated a common and potentially dangerous anomalous event present in many aviation accidents: unstable approaches. According to the FAA, an approach is considered unstable when at least one of several key variables related to energy management exceeds a predetermined threshold [29]. One common cause of an unstable approach is when an aircraft does not maintain a constant speed descent profile at several key distances and altitudes from the touchdown zone. According to the International Air Transport Association (IATA), 61% of the total accidents during the 2012-2016 period happened in the approach and landing phase of flight. Unstable approaches were determined to be a factor in 16% of those accidents [30]. Unstable approaches can result in hard landings, loss of aircraft control, runway excursions, and collision with terrain or infrastructure [31]. The cause of accidents in the presence of unstable approaches can be attributed any number of factors such as a lapse of aeronautical decision-making (ADM), inadequate crew resource management (CRM), or an aircraft malfunction, poor environmental conditions, etc. In this study, we investigate changes in the complexity of flight dynamics throughout various flight phases to yield actionable information that can be used to detect unstable approaches ahead of time.

The study of unstable approaches provides a foundation on which to analyze entropic methods and gain algorithmic insight, so that the methodology can be expanded to other risk scenarios discussed in the prior work. To this end, we propose and investigate the following research questions (RQs) in this paper:

RQ1 In addition to statistical features, can complexity features of flight dynamics characterize the flight phases between takeoff and landing?

RQ2 How do the entropy dynamics vary between stable and unstable approaches at different time instances before landing?

II. Methods

The main objective of our methodology was to study how entropy dynamics change over the course of a flight, especially during the approach phase of an aircraft. However, before the entropic analysis, the flight data had to be preprocessed to extract segments in the time series data relevant to our analysis. This preprocessing stage not only involved identifying the takeoff and landing points of a flight, but also labeling the flight approach as unstable or stable before the airplane landed. This section covers the preprocessing and entropic analysis in greater detail.

A. Dataset Preprocessing

In this study, we used the publicly available NASA Sample Flight Data, hereafter referred to as the NASA dataset, hosted on the NASA DASHlink public data-sharing platform [32]. The dataset contains de-identified flight recorded data of 180,000 commercial regional jet flights. Each flight file is saved in the MATLAB MAT binary format and contains 186 flight variables. These variables contain aircraft dynamics, flight parameters, and other system performance information of the aircraft. For example, critical aircraft information such as airspeed, altitude, and landing gear configuration can be found among the flight variables. Weather conditions, except wind shear warnings and wind speed, are excluded from the dataset. Additionally, the dataset exhibits a limited range of sampling frequencies. All flight variables are sampled between 0.25–16 Hz, with over 95% of the variables sampled at 4 Hz or below.

1. Identifying Takeoff and Landing

The first stage of the preprocessing phase required the identification of the time instances at which an aircraft took off and landed. In this study, an aircraft landing can refer to any of the following types of landing attempts: a successful touchdown, a landing rejected after touchdown, or a landing rejected in midair. The extraction of this segment in the time series was necessary for the experiments in the subsequent processing stages. The flight takeoff was identified by analyzing the flight phase variable and finding the instance at which the aircraft registered a takeoff. The identification of the flight landing required more steps, due to the fact that not all flights that took off registered an attempted landing during the approach phase. The most common reason for the lack of an attempted landing was incomplete data for a flight. Additionally, before the landing could be determined, flights with more than one approach phase required further filtering. Short approach phases lasting a couple of minutes were registered by the aircraft when it descended to make a small change to its cruising altitude. To ignore these short approach phases, two other flight variables were used. These variables were altitude (elevation of the destination airport acting as the reference) and weight-on-wheels. By using

altitude we were able to filter out approach phases where the plane did not fly below 1,000 ft. We selected this altitude threshold because it is used in the determination of an unstable approach under instrument flight rules (IFR) [1]. Once a valid approach phase was established, the weight-on-wheels variable was used to determine if the plane touched down during the approach phase. If the plane touched down, the point of touchdown was taken as the landing. If it did not touch down and the plane flight phase switched to climbing seconds later, we recorded a rejected landing and the lowest point in the plane's altitude was taken as the landing attempt.

Due to the low sampling rate (4 Hz or lower) of the majority of the signals, a median filter with a 10-second moving window was used to remove false readings and measurement dropouts. A fixed time was used for the window size instead of a fixed sample, due to the varying sampling rates of the flight variables. Any non-attenuated noise characteristics that remained after filtering were directly handled by the entropic methods. Additionally, in the preprocessing stage, flight variables used in the entropic analysis were upsampled to the highest sampling frequency of a signal in the set using linear interpolation.

2. Detecting Stable and Unstable Approaches

To determine whether a flight exhibited an unstable or stable approach, we investigated the top 3 predictor variables that are used to determine the presence of an unstable approach as listed in [33]. These variables were glideslope deviation (GLS), localizer deviation (LOC), and deviation between computed airspeed (CAS) and selected airspeed (CASS). Glideslope and localizer deviation form part of the radio navigation and instrument landing system (ILS) used during approach in conjunction with visual navigation under clear weather conditions. Localizer deviation provides horizontal alignment to the centerline of the runway during approach, while glideslope deviation provides vertical alignment of the descent profile so that a $3°$ descent profile is maintained throughout the approach as per FAA regulations. Airspeed deviation (CAS-CASS) from a set reference value is used to determine if the plane is descending too slowly or too quickly. The exceedance rules for determining an unstable approach can be found in a briefing published by the Flight Safety Foundation [34]. Using these exceedance thresholds, flights in the NASA dataset were labeled as stable or unstable at the 1,000 ft altitude mark (height above runway). The variables that caused the instability were also noted during the labeling process.

B. Entropic Analysis

With the time series segments between takeoff and landing obtained in the preprocessing stage, as well as the identification of an unstable or stable approach, here we define the functions used in the entropic analysis to characterize the flight dynamics. The entropic analysis consisted of two different experiments, with the goal of each experiment to provide an answer to one of our RQs. The flight dynamics we analyzed were altitude, glideslope deviation, localizer deviation, and airspeed deviation.

1. Complexity Measures

The entropic analysis of flight dynamics relies on two methods to measure signal complexity: sample entropy and permutation entropy. Both of these entropic measures have been used to characterize complex, nonlinear dynamical systems in biomedical and financial applications [35, 36]. At their core, both complexity measures quantify the degree of self-similarity exhibited at different scales in a time series. A signal containing regular and similar patterns will tend to produce a low entropy measurement, while more complex and unpredictable patterns will yield a higher entropy measurement. The measurement produced by sample entropy when applied to a time series is governed by two parameters: the embedding dimension m and the tolerance r. Formally, given a time series $x = \{x_t : t = 1, \ldots, T\}$, we define a template vector with length m as $X_m(i) = \{x_i, x_{i+1}, x_{i+2}, \ldots, x_{i+m-1}\}$ and a distance function $d[X_m(i), X_m(j)]_{i \neq j}$. With this, sample entropy is defined as

$$\text{SampEn}(x, m, r) = -\ln\left(\frac{A}{B}\right), \tag{1}$$

where A is the number of $d[X_m(i), X_m(j)] < r$ and B is the number of $d[X_{m+1}(i), X_{m+1}(j)] < r$. Unless otherwise stated, the distance function d used is the Chebyshev function, $m = 3$, and $r = 0.18\sigma_x$, where σ_x is the standard deviation of the time series x. This choice of parameters was made in an informed manner according to the guidelines provided in [37]. Additionally, due to the dependence on the standard deviation of the signal in the sample entropy calculation, the signals were detrended by taking their first-order difference prior to calling the entropy function. This

reduces the likelihood of low complexity trends masking more complex state changes in a signal, thereby producing a low complexity measurement.

To define permutation entropy, we continue from the definition of the time series x. Similar to sample entropy, permutation entropy relies on an embedding parameter m to define an embedding vector at every time step i with the same construction as the vector $X_m(i)$ used in sample entropy. However, instead of comparing the distance of vector pairs to a tolerance level r, permutation entropy counts the number of permutation patterns present in the embedding vector. Formally,

$$\text{PermEn}(x, m, \tau) = -\sum_{j=1}^{m!} \pi_j \ln(\pi_j),$$ (2)

where π_i is the frequency of the i-th permutation pattern in the vector $X_m(i)$, $m!$ is the total number of possible permutations, and τ is the embedding delay parameter that can be used to create embedding vectors with non-consecutive points such that for $\tau \geq 1$, $X_m(i) = \{x_i, x_{i+\tau}, x_{i+2\tau}, \dots\}$. To expand on the notion of permutation patterns, take the example of a time series $x = \{2, 7, 1, 8, 2\}$, with $m = 3$ and $\tau = 1$. When $i = 1$, $X_3(1) = \{2, 7, 1\}$, this yields $\{1, 2, 7\}$ when $X_3(1)$ is sorted in ascending order. Thus, the third element in $X_3(1)$ is moved to the first position in the sorted vector, the first element is moved to the second position, and the second element is moved to the last position, thereby creating the permutation $(3, 1, 2)$ and incrementing the count of π_j, for some j, by 1. This procedure is followed for the remaining embedding vectors to arrive at the frequencies $\{\pi_j\}_{j=1}^{m!}$. We followed the practical recommendations found in [26] and used the parameters $m = 3$ and $\tau = 1$, unless otherwise noted.

2. Characterzing Flight Phases Between Takeoff and Landing Using k-Means Clustering

The study of RQ1 required the calculation of complexity and statistical measurements between the takeoff and landing stages of a flight. The flight dynamics we analyzed were altitude (ALT) and airspeed deviation (CAS-CASS). The glideslope deviation and localizer deviation variables analyzed for RQ2 were omitted from this analysis due to their near exclusive use during the approach phase, when the antenna array at the destination airport is able to provide a strong signal lock-on as the airplane approaches the runway. By studying altitude and airspeed deviation, we hypothesized that complexity in the dynamics of the aircraft due to turbulence or other unknown factors, especially during climb and approach, would translate to unpredictable changes in altitude and airspeed deviation. The complexity of the flight variables was calculated every 15 seconds over a 60-second rolling window, with 45 seconds of overlap with the previous window. The 60-second window provided approximately 240 samples at a sampling rate of 4 Hz, which was above the recommended minimum of 100 samples for a valid entropy estimate by sample entropy and permutation entropy [38]. The three main flight phases present between takeoff and landing that we sought to characterize were the climb, cruise, and approach phases. To gain a full description of the complexity of the flight dynamics during a flight, we also calculated the standard deviation and mean of each rolling window. Thus, for each signal, the three features derived from the entropic and statistical analysis were complexity, mean, and standard deviation. A random sample of approximately 3,000 flights from the NASA dataset was used to generate these features. In total, 890,000 measurements were individually produced for entropy, standard deviation, and mean. This translated to an average of 300 rolling windows per flight, which at the rate of one window every 15 seconds, resulted in a mean flight time of 75 minutes from takeoff to landing.

Following the feature generation, k-means clustering was used to identify states from the distributions of the features. Due to the use of two different complexity measures, sample entropy and permutation entropy, on two flight variables, we evaluated the "quality" of the k-means clustering using the Davies-Bouldin index (DBI). The DBI was calculated over a cluster range of 1 through 5 for each complexity measure and flight variable. The number of clusters corresponding to the lowest DBI was used in the clustering of the flight variables. After clustering, the states (i.e., clusters) were overlaid on the altitude plot of a random selection of flights that were not part of the cluster training, in order visualize when the states occurred throughout the duration of flights.

3. Multiscale Entropic Analysis During Approach Phase

We performed a multiscale entropic analysis to determine a statistical difference in the entropy dynamics between flights with unstable approaches and flights with stable approaches. Multiscale entropy relies on an entropy function, such as sample entropy or permutation entropy, and a scale factor δ to downsample the signal at every δ points and, effectively, compute the entropy of a time series at different temporal scales. Every successive downsampling iteration removes slow trends in the signal, so that the entropy function can measure the complexity of the remaining
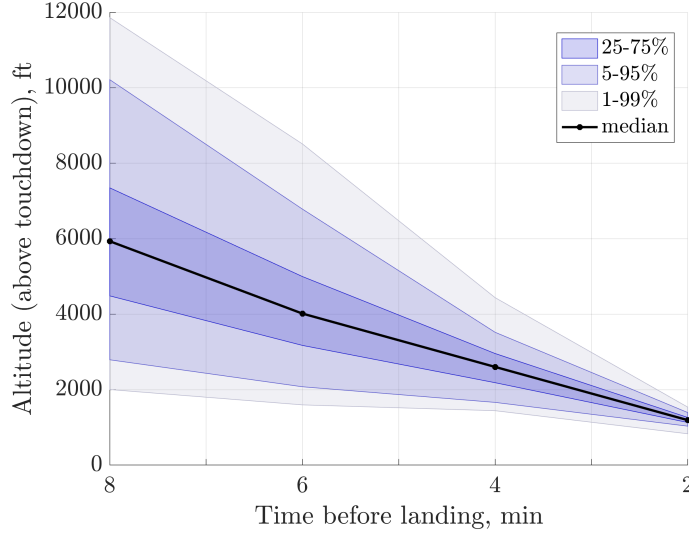
Fig. 1 Altitude distribution percentiles of flights with stable approaches. The median altitude 2 minutes before touchdown is approximately 1,200 ft.

non-attenuated irregular trends. Highly complex signals will exhibit high entropy measurements over a wide range of temporal scales, with the entropy measurements decreasing or increasing as δ grows, depending on the entropy function. Careful consideration was given to the selection of scales to avoid going well under the threshold of 100 samples when downsampling the signal at high scales. Therefore, the first experiment characterized the complexity of unstable approach predictor variables in 2 minute increments before a successful or rejected landing. The largest time window of 8 minutes overlapped the smaller time windows of 6, 4, and 2 minutes before landing. Each successively larger, overlapping time window allowed 3 more scales to be studied. At the smallest time window of 2 minutes, the minimum number of samples used was 80 samples, which corresponded to the third temporal scale. This 2-minute window coincided with the median altitude of 1,200 ft during stable approaches (see Fig. 1), which is close to the 1,000 ft threshold for determining an unstable approach. We note that for unstable approaches, regardless of the variable causing the instability, the altitude median tended to be higher than that of stable approaches. In summary, the first multiscale entropy experiment used sample entropy and permutation entropy to characterize the complexity of flight variables at 2 minutes (3 scales), 4 minutes (6 scales), 6 minutes (9 scales), and 8 minutes (12 scales) before landing.

Whereas the main objective of the first experiment was to uncover the presence high entropy dynamics at large scales that can be used to differentiate unstable and stable approaches, the second multiscale experiment was designed to uncover how the entropy dynamics evolved over several stages (i.e., time windows) of the approach phase. Instead of creating overlapping time windows, four non-overlapping 2-minute windows were created that encompassed a total time of 8 minutes before a successful or rejected landing took place. This resulted in time windows at 0–2, 2–4, 4–6, and 6–8 minutes before landing. The maximum temporal scale analyzed in the complexity calculation of each window was 3. Again, the selection of the maximum scale was guided by the need to maintain around 100 samples after each downsampling iteration. Following both experiments, a two-sided Wilcoxon rank sum test was conducted between flights with unstable approaches and flights with stable approaches (for a given time window before landing, scale factor, and predictor variable). The use of a rank sum test was due to the non-normal complexity distribution of the predictor variables.

III. Results

The resulting figures and tables of the entropic analysis are grouped according to the research question (RQ) they aim to answer. Results related to the flight phases and the states identified by k-means clustering are tied to RQ1, whereas the multiscale entropy analysis results are tied to RQ2. These groupings help structure the Discussion section.

A. Characterizing Flight Phases Through Clustering

The characterization of the climb, cruise, and approach phases using k-means clustering is shown in Figs. 2 and 3. Both figures show the clusters generated when mean, standard deviation (SD), and entropy are used as the flight variable features. The former figure uses sample entropy while the latter uses permutation entropy. The use of entropy, in addition to mean and SD, provides an augmented view of the statistical and entropic distribution of a flight variable's dynamics. We note the presence of outliers with high complexity values in the altitude clusters in Fig. 2 (left). For airspeed deviation (right plot), these outliers are sufficiently separated from the main group of clusters that they are grouped into their own cluster. This is not the case for the altitude clustering in the left plot. Moreover, whereas the cluster boundaries for altitude lie along the mean axis, the airspeed deviation cluster boundaries lie along the complexity axis. Similarly, in Fig. 3, the altitude cluster boundaries lie along the mean axis. However, the airspeed deviation cluster boundaries lie along the standard deviation axis. Clear outlier groups are not present in the results for permutation entropy.

For altitude (ALT) the DBI (Davies-Bouldin index) indicated the use of 3 clusters with both sample entropy and permutation entropy. For airspeed deviation (CAS-CASS), the DBI yielded 4 clusters for sample entropy and 2 for permutation entropy. The fourth cluster for airspeed deviation and sample entropy is solely for the outliers. From the differences in the number of clusters produced, outliers, and distribution of points within clusters, we can visually observe a notable difference between sample entropy and permutation entropy for both variables. Insight into these differences is provided in the Discussion.
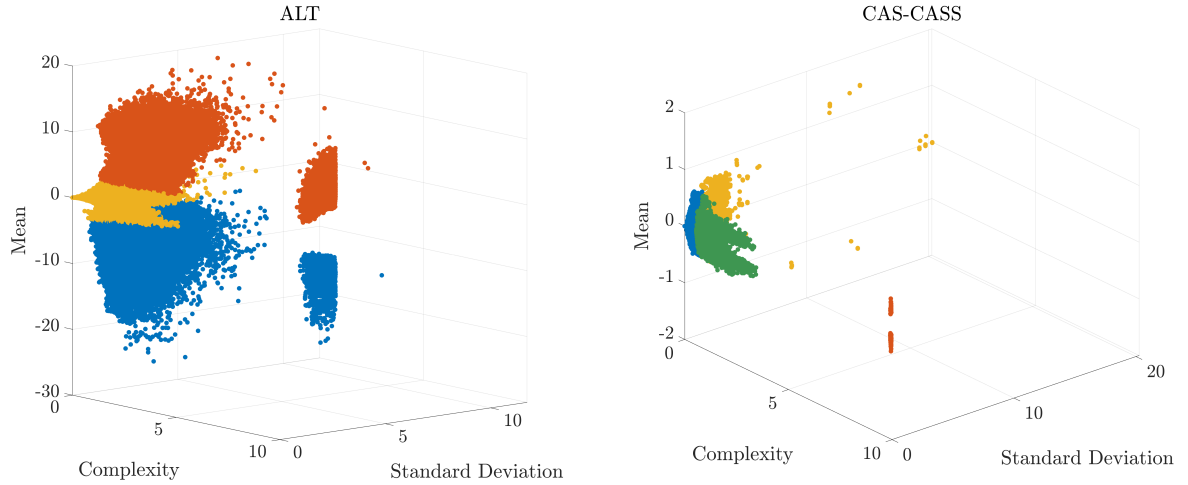

Fig. 2 Clusters produced by k-means using complexity and statistical features of (left) altitude and (right) airspeed deviation. The complexity measure used was sample entropy.

In addition to the states (i.e., clusters) identified through k-means clustering, Figs. 4 and 5 show where the states occur between takeoff and landing. The figures show the original flight variable in black and the states overlaid on the flight variable. The colors of the states correspond to the colors of the clusters in Figs. 2 and 3. We further note the absence of the outlier (red) state in the three flights in Fig. 4(b). Visually, the 3 phases of flight we analyzed (climb, cruise, and approach) can be distinctly identified through the grouping of the states in the altitude plots. This state grouping is less structured in airspeed deviation due in part to the fewer states identified, as in the case of Fig. 5(b).

B. Multiscale Entropic Analysis of Stable and Unstable Approaches

The results of the multiscale entropic analysis during the approach phase are grouped by the unstable approach predictor variables. These predictor variables were glideslope deviation (GLS), localizer deviation (LOC), and computed airspeed deviation from selected airspeed (CAS-CASS). Each figure in Figs. 6 to 11 shows the entropy (mean ± standard error) at different temporal scales. The subplot on the left of the figure is for the overlapping time windows and the subplot on the right of the figure is for the non-overlapping windows. Within each subplot, the results for stable and unstable approaches are presented for different time windows.

Additionally, the tables in Tables 1 to 4 provide a different view of the entropy statistics. Within them, more precise
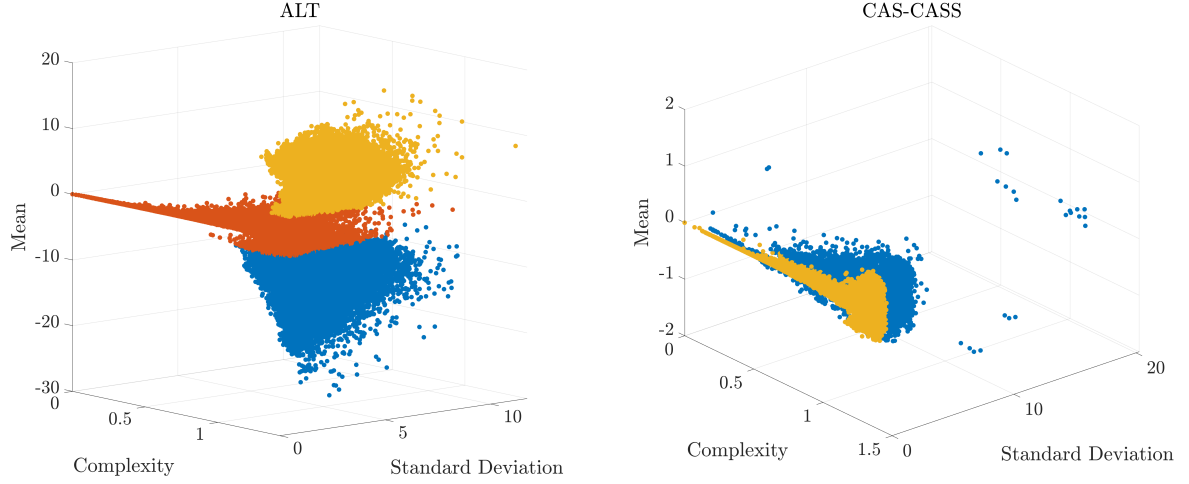
Fig. 3 **Clusters produced by k-means using complexity and statistical features of (left) altitude and (right) airspeed deviation. The complexity measure used was permutation entropy.**
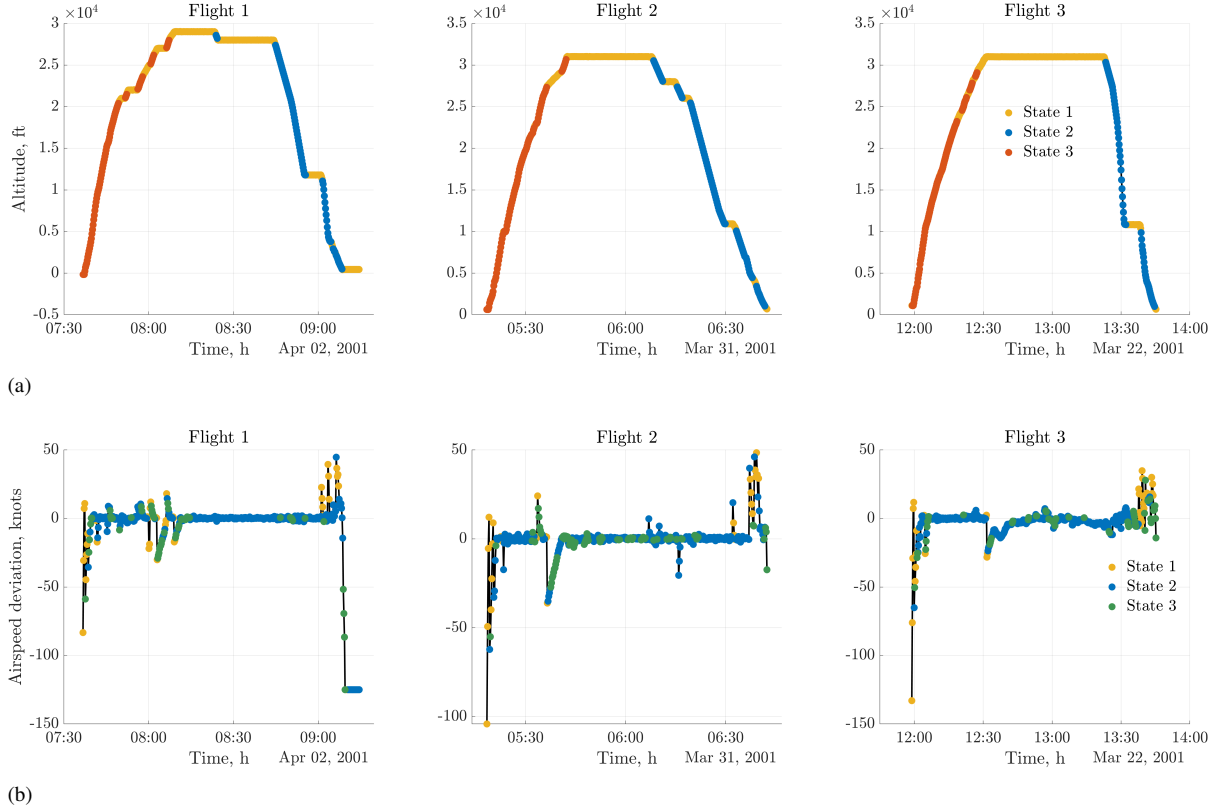

(a)

(b)

Fig. 4 **Occurrence of (a) altitude and (b) airspeed deviation states identified by k-means clustering between takeoff and landing. The complexity measure used was sample entropy.**

measurements of the mean and standard error between the stable approach and unstable approach distributions can be found. If the null hypothesis of the Wilcoxon rank sum test was rejected, a $p < 0.01$ is indicated by a * and a $p < 0.05$ in the Significance column. Temporal scales that were not analyzed due to a shortage of samples in a time window are denoted by a solid dashed line. Each table provides the sample entropy and permutation entropy results for a single
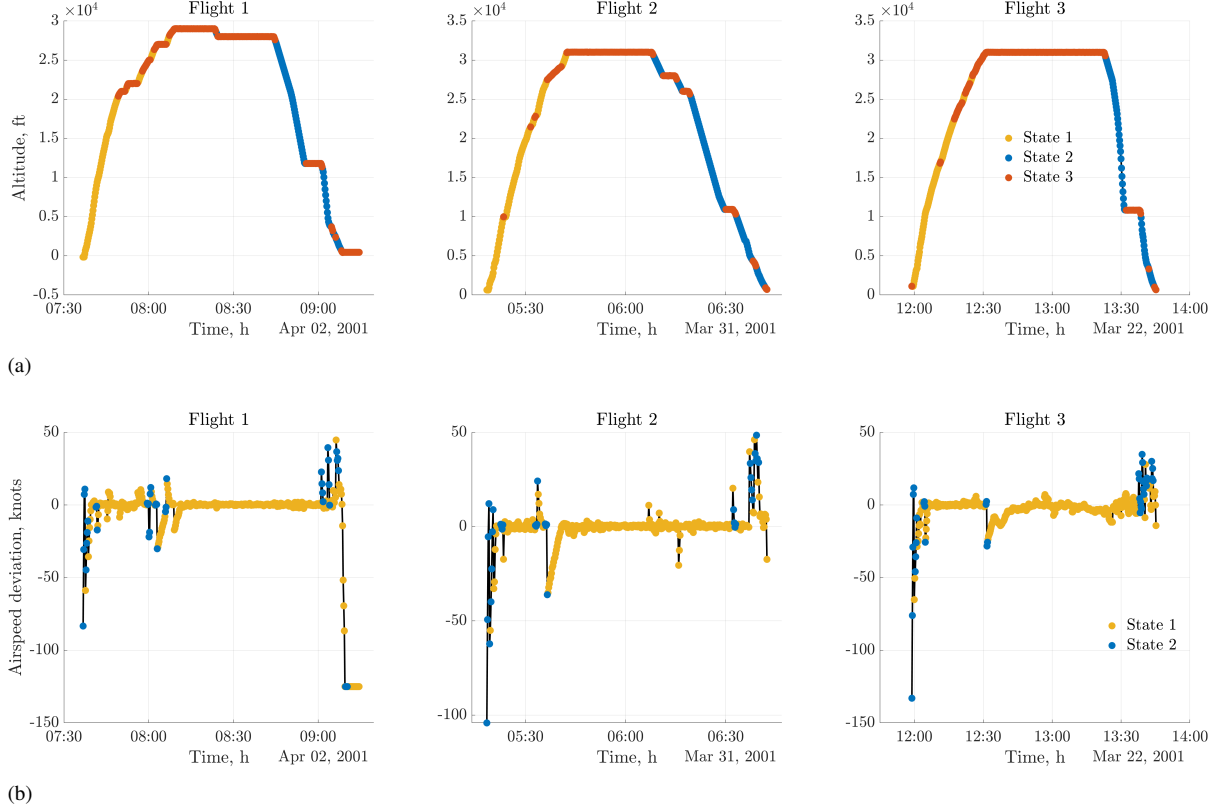
Fig. 5   Occurrence of (a) altitude and (b) airspeed deviation states identified by k-means clustering between takeoff and landing. The complexity measure used was permutation entropy.

unstable approach predictor variable. The tables for LOC and CAS-CASS multiscale sample entropy statistics were omitted for the overlapping windows, as all unstable and stable approach distributions were statistically different at a $p < 0.01$. The following descriptions provide more detail on the multiscale results.

1. Glideslope Deviation

   The glideslope deviation multiscale entropy results shown in Fig. 6 depict a clear upward trend in the complexity as the temporal scale increases. This trend is contrasted by the downward tendency after the third temporal scale in the multiscale permutation results in Fig. 7. Furthermore, in Table 1, there does not exist a statistically significant difference in the sample entropy distributions for the last two temporal scales in the non-overlapping window starting at 6 minutes prior to landing. This same observation is not valid to the same extent across all non-overlapping windows for permutation entropy. However, the non-overlapping windows for permutation entropy do not show an established pattern (e.g., unstable complexity greater than stable complexity, or vice versa) across all temporal scales. This consistency *is* exhibited in sample entropy in both the overlapping and non-overlapping windows.

2. Localizer Deviation

   The complexity distributions for localizer deviation in Figs. 8 and 9 exhibit patterns similar to those found in glideslope deviation. That is, sample entropy (for both types of time windows) shows an upward tendency as the temporal scale increases while permutation entropy shows an upward and then downward trend, but mainly in the overlapping windows. In contrast to glideslope, however, stable approaches show a higher sample entropy than unstable approaches across almost all temporal scales in the overlapping windows. This pattern is also visible in the non-overlapping windows, but only for the 2-minute and 4-minute windows. Another difference between glideslope and localizer deviation is the greater permutation entropy separation between unstable and stable approaches at the third temporal scale in the non-overlapping windows. However, all separations at the third temporal scale for both permutation and sample entropy
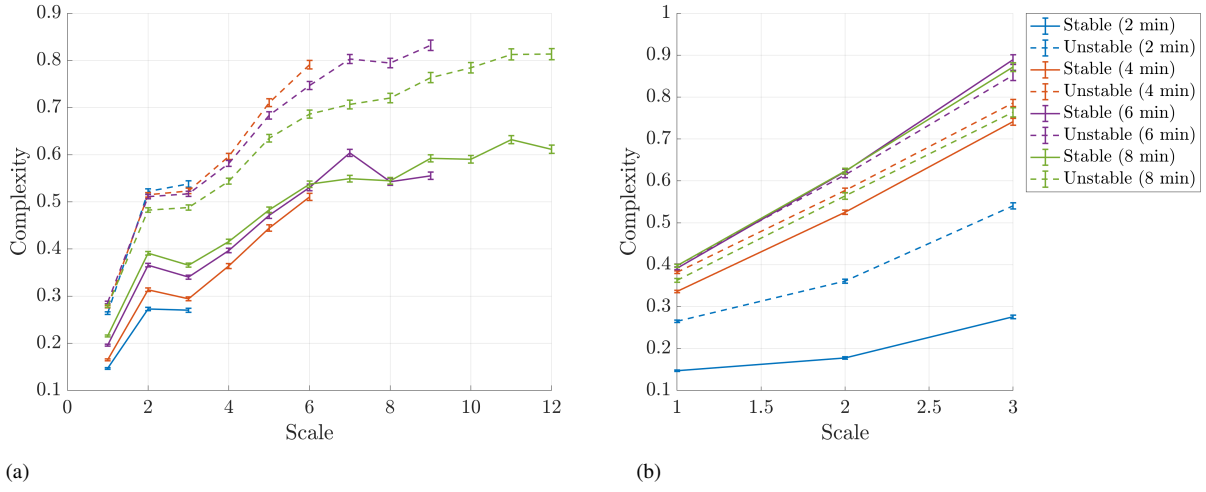
9

Fig. 6 Multiscale sample entropy for glideslope deviation, GLS (mean ± std. error). (Left) overlapping time windows and (right) non-overlapping time windows before landing.
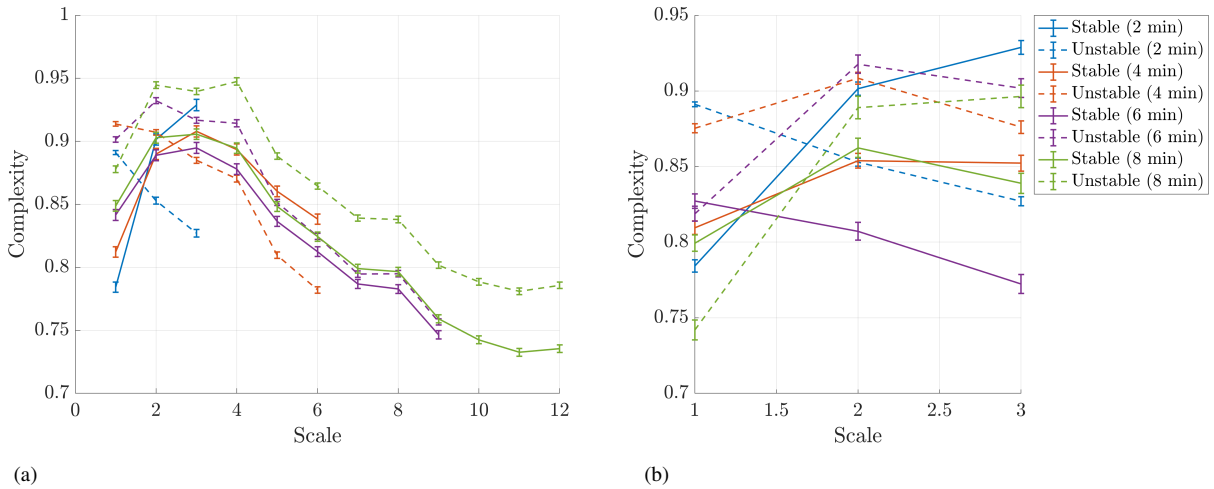

Fig. 7 Multiscale permutation entropy for glideslope deviation, GLS (mean ± std. error). (Left) overlapping time windows and (right) non-overlapping time windows before landing.

were statistically significant in the non-overlapping windows as summarized in Table 2.

3. Airspeed Deviation

The multiscale entropy results for airspeed deviation exhibited different patterns in the permutation entropy distributions (Figs. 10 and 11) compared to glideslope and localizer deviation. Instead of the upward and then downward trend found in glideslope and localizer deviation, the permutation entropy tended to decrease as the temporal scale increased in both overlapping and non-overlapping windows. Similar to localizer deviation, stable approaches again had higher sample entropy values than unstable approaches, at least in the overlapping windows. This trend was only present in the 2-minute non-overlapping window for sample entropy. All differences in unstable and stable approaches were statistically significant across all scales for overlapping windows, and across all temporal scales for non-overlapping windows, except for the windows starting at 8 minutes (see Table 3).

10

Table 1 **Glideslope deviation (GLS) multiscale entropy statistics (mean ± std. error) for non-overlapping time windows before landing (*:** $p < 0.01$**, **:** $p < 0.05$**).**

Sample Entropy

Time Window (2-Minute Windows Starting at Specified Time Before Landing)

	2 min			4 min		
Scale	Stable	Unstable	Significance	Stable	Unstable	Significance
1	$0.15 \pm 1.8 \times 10^{-3}$	$0.27 \pm 2.7 \times 10^{-3}$	*	$0.34 \pm 2.7 \times 10^{-3}$	$0.38 \pm 3.1 \times 10^{-3}$	*
2	$0.18 \pm 2.8 \times 10^{-3}$	$0.36 \pm 4.9 \times 10^{-3}$	*	$0.53 \pm 5.2 \times 10^{-3}$	$0.58 \pm 5.6 \times 10^{-3}$	*
3	$0.28 \pm 4.1 \times 10^{-3}$	$0.54 \pm 7.1 \times 10^{-3}$	*	$0.74 \pm 8.1 \times 10^{-3}$	$0.79 \pm 8.3 \times 10^{-3}$	*

	6 min			8 min		
Scale	Stable	Unstable	Significance	Stable	Unstable	Significance
1	$0.39 \pm 3.2 \times 10^{-3}$	$0.40 \pm 3.8 \times 10^{-3}$	*	$0.40 \pm 3.8 \times 10^{-3}$	$0.36 \pm 4.5 \times 10^{-3}$	*
2	$0.62 \pm 6.0 \times 10^{-3}$	$0.61 \pm 6.6 \times 10^{-3}$		$0.62 \pm 6.7 \times 10^{-3}$	$0.56 \pm 7.7 \times 10^{-3}$	*
3	$0.89 \pm 12 \times 10^{-3}$	$0.85 \pm 12 \times 10^{-3}$		$0.87 \pm 10 \times 10^{-3}$	$0.76 \pm 11 \times 10^{-3}$	*

Permutation Entropy

Time Window (2-Minute Windows Starting at Specified Time Before Landing)

	2 min			4 min		
Scale	Stable	Unstable	Significance	Stable	Unstable	Significance
1	$0.78 \pm 4.1 \times 10^{-3}$	$0.89 \pm 1.6 \times 10^{-3}$	*	$0.81 \pm 4.4 \times 10^{-3}$	$0.87 \pm 2.9 \times 10^{-3}$	*
2	$0.90 \pm 4.4 \times 10^{-3}$	$0.85 \pm 2.7 \times 10^{-3}$	*	$0.85 \pm 4.9 \times 10^{-3}$	$0.91 \pm 3.9 \times 10^{-3}$	*
3	$0.93 \pm 4.5 \times 10^{-3}$	$0.83 \pm 3.0 \times 10^{-3}$	*	$0.85 \pm 5.2 \times 10^{-3}$	$0.88 \pm 4.2 \times 10^{-3}$	**

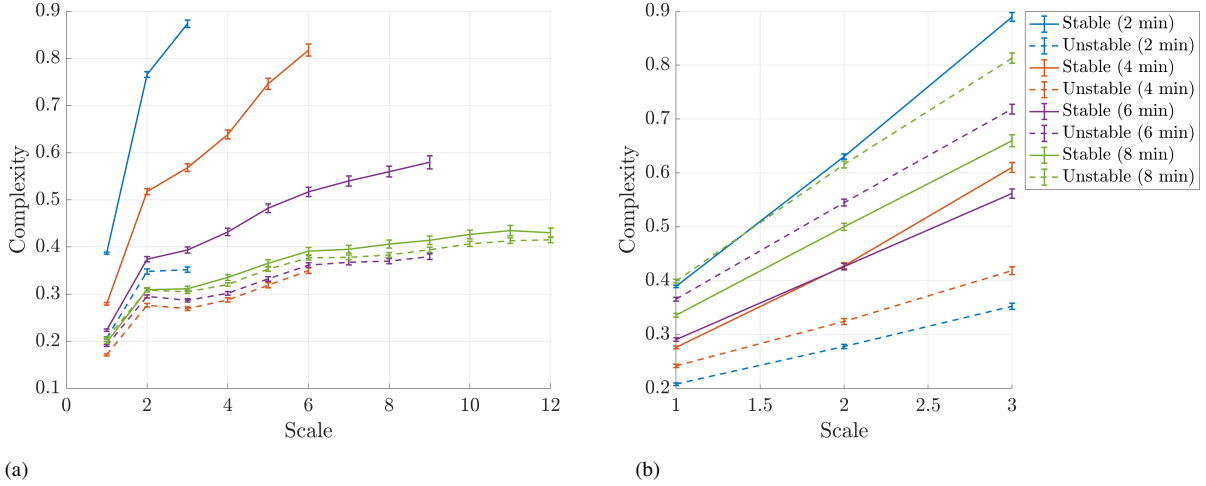|	6 min			8 min		
Scale	Stable	Unstable	Significance	Stable	Unstable	Significance
1	$0.83 \pm 4.8 \times 10^{-3}$	$0.82 \pm 4.9 \times 10^{-3}$		$0.80 \pm 5.4 \times 10^{-3}$	$0.74 \pm 6.5 \times 10^{-3}$	*
2	$0.81 \pm 5.9 \times 10^{-3}$	$0.92 \pm 6.0 \times 10^{-3}$	*	$0.86 \pm 6.4 \times 10^{-3}$	$0.89 \pm 7.5 \times 10^{-3}$	*
3	$0.77 \pm 6.3 \times 10^{-3}$	$0.90 \pm 6.2 \times 10^{-3}$	*	$0.84 \pm 6.6 \times 10^{-3}$	$0.90 \pm 7.4 \times 10^{-3}$	*

(a)   (b)

Fig. 8 **Multiscale sample entropy for localizer deviation, LOC (mean ± std. error). (Left) overlapping time windows and (right) non-overlapping time windows before landing.**

IV. Discussion

RQ1: Characterizing Flight Phases by Incorporating Entropy Dynamics

 Figs. 2 and 3 revealed the most important features needed to characterize the evolution of a flight variable throughout takeoff and landing. For example, for both sample entropy and permutation entropy, the cluster boundaries for altitude lie along the mean axis. This observation is in agreement with how altitude complexity is calculated using sample entropy; that is, because the first order differences of the altitude (i.e., altitude rate) act as the input to the sample entropy
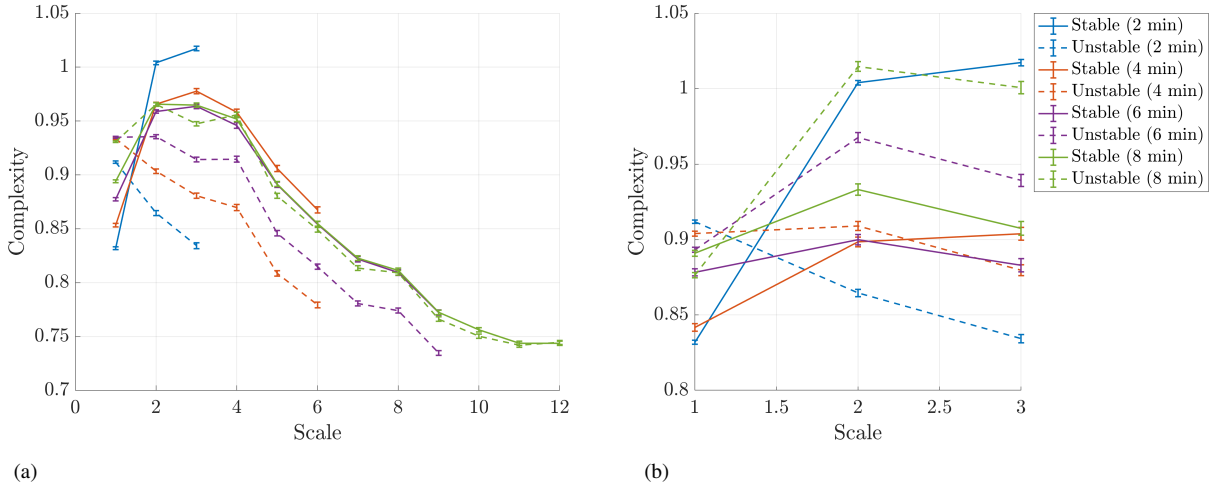
(a)   (b)

Fig. 9   Multiscale permutation entropy for localizer deviation, LOC (mean ± std. error). (Left) overlapping time windows and (right) non-overlapping time windows before landing.

Table 2   Localizer deviation (LOC) multiscale entropy statistics (mean ± std. error) for non-overlapping time windows before landing (*: $p < 0.01$, **: $p < 0.05$).

	Sample Entropy					
	Time Window (2-Minute Windows Starting at Specified Time Before Landing)					
	2 min			**4 min**		
Scale	Stable	Unstable	Significance	Stable	Unstable	Significance
1	$0.39 \pm 2.2 \times 10^{-3}$	$0.21 \pm 2.4 \times 10^{-3}$	*	$0.28 \pm 2.7 \times 10^{-3}$	$0.24 \pm 3.2 \times 10^{-3}$	*
2	$0.63 \pm 4.7 \times 10^{-3}$	$0.28 \pm 3.9 \times 10^{-3}$	*	$0.43 \pm 5.5 \times 10^{-3}$	$0.32 \pm 5.4 \times 10^{-3}$	*
3	$0.89 \pm 8.3 \times 10^{-3}$	$0.35 \pm 5.7 \times 10^{-3}$	*	$0.61 \pm 9.1 \times 10^{-3}$	$0.42 \pm 7.3 \times 10^{-3}$	*
	6 min			**8 min**		
Scale	Stable	Unstable	Significance	Stable	Unstable	Significance
1	$0.29 \pm 3.1 \times 10^{-3}$	$0.37 \pm 3.5 \times 10^{-3}$	*	$0.34 \pm 3.6 \times 10^{-3}$	$0.40 \pm 3.4 \times 10^{-3}$	*
2	$0.43 \pm 5.8 \times 10^{-3}$	$0.54 \pm 6.3 \times 10^{-3}$	*	$0.50 \pm 6.7 \times 10^{-3}$	$0.62 \pm 6.4 \times 10^{-3}$	*
3	$0.56 \pm 8.6 \times 10^{-3}$	$0.72 \pm 9.1 \times 10^{-3}$	*	$0.66 \pm 11 \times 10^{-3}$	$0.81 \pm 9.3 \times 10^{-3}$	*
	Permutation Entropy					
	Time Window (2-Minute Windows Starting at Specified Time Before Landing)					
	2 min			**4 min**		
Scale	Stable	Unstable	Significance	Stable	Unstable	Significance
1	$0.83 \pm 1.3 \times 10^{-3}$	$0.91 \pm 1.1 \times 10^{-3}$	*	$0.84 \pm 2.5 \times 10^{-3}$	$0.90 \pm 1.6 \times 10^{-3}$	*
2	$1.0 \pm 1.6 \times 10^{-3}$	$0.86 \pm 2.4 \times 10^{-3}$	*	$0.90 \pm 3.2 \times 10^{-3}$	$0.91 \pm 2.9 \times 10^{-3}$	
3	$1.0 \pm 2.1 \times 10^{-3}$	$0.83 \pm 2.8 \times 10^{-3}$	*	$0.90 \pm 4.2 \times 10^{-3}$	$0.88 \pm 3.5 \times 10^{-3}$	*
	6 min			**8 min**		
Scale	Stable	Unstable	Significance	Stable	Unstable	Significance
1	$0.88 \pm 2.3 \times 10^{-3}$	$0.89 \pm 1.7 \times 10^{-3}$		$0.89 \pm 1.9 \times 10^{-3}$	$0.88 \pm 1.7 \times 10^{-3}$	*
2	$0.90 \pm 3.4 \times 10^{-3}$	$0.97 \pm 3.3 \times 10^{-3}$	*	$0.93 \pm 3.8 \times 10^{-3}$	$1.0 \pm 3.2 \times 10^{-3}$	*
3	$0.88 \pm 4.4 \times 10^{-3}$	$0.94 \pm 4.0 \times 10^{-3}$	*	$0.91 \pm 4.6 \times 10^{-3}$	$1.0 \pm 4.0 \times 10^{-3}$	*

function, the altitude rate will be positive during the climb phase, near zero during cruise, and negative during approach. Thus, the mean will have the largest feature variation and influence the k-means algorithm to place clusters along its axis. This clustering result is validated by the row of subplots in Fig. 4(a), where we observe the positive mean, red cluster at the beginning of the flights and the negative mean, blue cluster at the end of the flights. This pattern also holds for altitude clustering using permutation entropy in Fig. 5(a) (ignoring the color swap of the clusters). These state groupings are occasionally interrupted when the aircraft levels off during climb or approach and the altitude rate
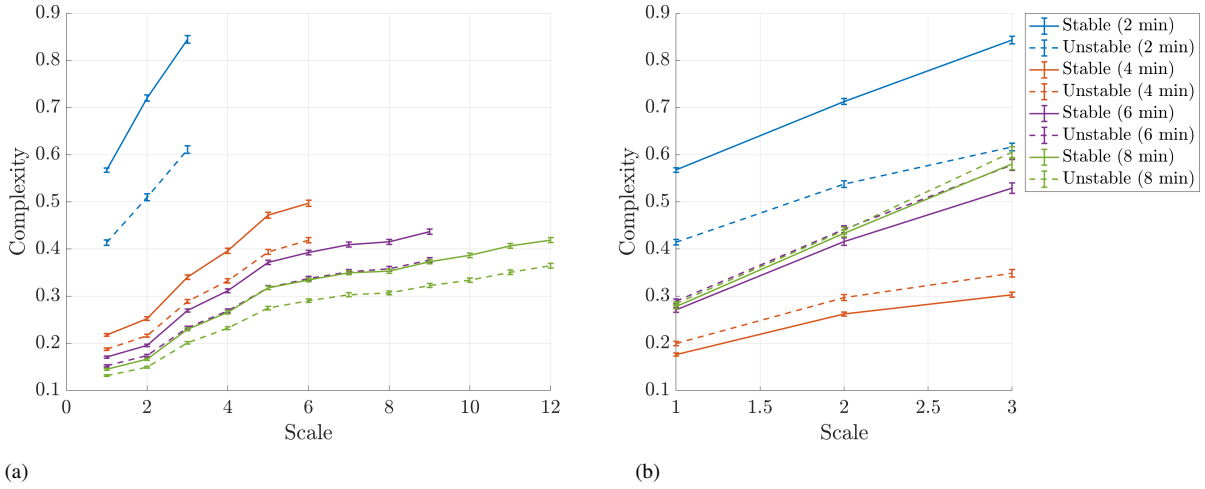
Fig. 10 Multiscale sample entropy for airspeed deviation, CAS-CASS (mean ± std. error). (Left) overlapping time windows and (right) non-overlapping time windows before landing.
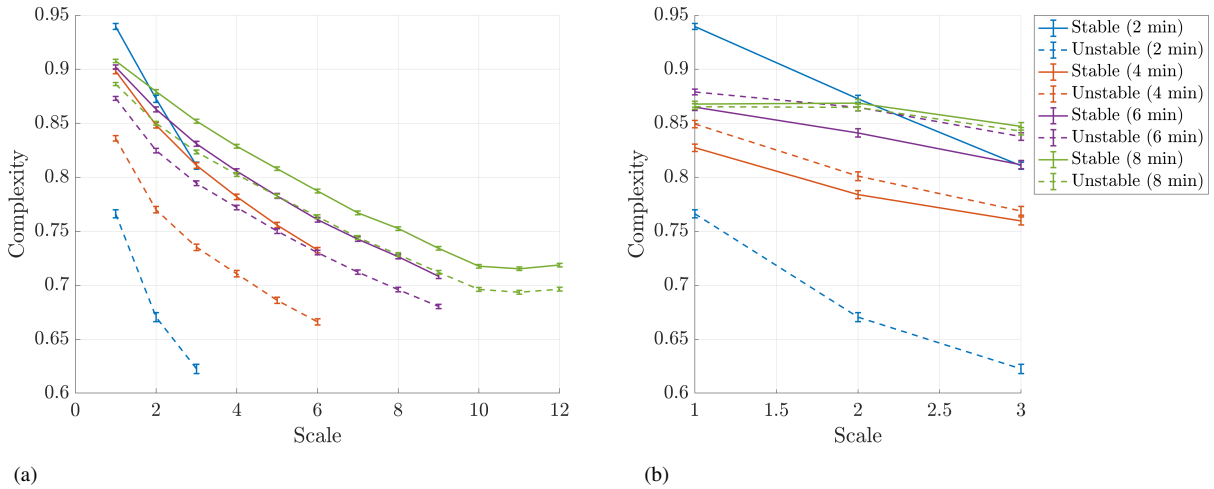

Fig. 11 Multiscale permutation entropy for airspeed deviation, CAS-CASS (mean ± std. error). (Left) overlapping time windows and (right) non-overlapping time windows before landing.

registers values close to zero. Further analysis into the high altitude complexity outliers observed in Fig. 2 revealed the cause of the outliers. These outliers occurred during periods of high altitude rate of change, which tends to occur during the climb phase of the flight as the airplane climbs to cruising speed or during the approach phase as the airplane descends periodically to get ready for landing. These periods of high ascent or descent rate resulted in high complexity values. However, this high complexity was not enough to warrant a separate cluster for the outliers.

Airspeed deviation did not exhibit the same degree of state grouping along the flight phases as altitude did, though there is evidence of rapid state changes (in the scale of minutes) near takeoff and landing (see Fig. 4(b) and Fig. 5(b)), where the greatest airspeed deviation occurs. These state changes are more clearly visible for permutation entropy, due to the use of only two states. These two states represent a low standard deviation (SD) in airspeed deviation during cruise, and a mixture of low SD and high SD during climb and cruise. Therefore, although airspeed may not be appropriate to uniquely determine each flight phase, it may be useful in determining if the aircraft is either climbing or in approach.

To summarize the results of the analysis for RQ1, the difference in the number of clusters and the direction of the

Table 3 **Airspeed deviation (CAS-CASS) multiscale entropy statistics (mean ± std. error) for non-overlapping time windows before landing (*: $p < 0.01$, **: $p < 0.05$).**

		Sample Entropy				
	Time Window (2-Minute Windows Starting at Specified Time Before Landing)					
	2 min			**4 min**		
Scale	Stable	Unstable	Significance	Stable	Unstable	Significance
1	$0.57 \pm 4.6 \times 10^{-3}$	$0.41 \pm 5.7 \times 10^{-3}$	*	$0.18 \pm 3.1 \times 10^{-3}$	$0.20 \pm 4.4 \times 10^{-3}$	
2	$0.71 \pm 6.4 \times 10^{-3}$	$0.54 \pm 7.0 \times 10^{-3}$	*	$0.26 \pm 4.3 \times 10^{-3}$	$0.30 \pm 6.3 \times 10^{-3}$	
3	$0.84 \pm 7.9 \times 10^{-3}$	$0.62 \pm 8.2 \times 10^{-3}$	*	$0.30 \pm 5.1 \times 10^{-3}$	$0.35 \pm 8.0 \times 10^{-3}$	**
	6 min			**8 min**		
Scale	Stable	Unstable	Significance	Stable	Unstable	Significance
1	$0.27 \pm 5.0 \times 10^{-3}$	$0.29 \pm 4.9 \times 10^{-3}$	*	$0.28 \pm 4.7 \times 10^{-3}$	$0.28 \pm 4.4 \times 10^{-3}$	
2	$0.42 \pm 8.0 \times 10^{-3}$	$0.44 \pm 7.6 \times 10^{-3}$	*	$0.43 \pm 7.6 \times 10^{-3}$	$0.44 \pm 7.1 \times 10^{-3}$	
3	$0.53 \pm 11 \times 10^{-3}$	$0.58 \pm 12 \times 10^{-3}$	*	$0.58 \pm 12 \times 10^{-3}$	$0.61 \pm 12 \times 10^{-3}$	**
		Permutation Entropy				
	Time Window (2-Minute Windows Starting at Specified Time Before Landing)					
	2 min			**4 min**		
Scale	Stable	Unstable	Significance	Stable	Unstable	Significance
1	$0.94 \pm 2.8 \times 10^{-3}$	$0.77 \pm 3.7 \times 10^{-3}$	*	$0.83 \pm 3.5 \times 10^{-3}$	$0.85 \pm 3.4 \times 10^{-3}$	*
2	$0.87 \pm 3.3 \times 10^{-3}$	$0.67 \pm 4.2 \times 10^{-3}$	*	$0.78 \pm 3.8 \times 10^{-3}$	$0.80 \pm 4.0 \times 10^{-3}$	*
3	$0.81 \pm 3.4 \times 10^{-3}$	$0.62 \pm 4.2 \times 10^{-3}$	*	$0.76 \pm 3.8 \times 10^{-3}$	$0.77 \pm 4.1 \times 10^{-3}$	**
	6 min			**8 min**		
Scale	Stable	Unstable	Significance	Stable	Unstable	Significance
1	$0.87 \pm 3.2 \times 10^{-3}$	$0.88 \pm 2.7 \times 10^{-3}$	**	$0.87 \pm 2.7 \times 10^{-3}$	$0.87 \pm 2.5 \times 10^{-3}$	
2	$0.84 \pm 3.8 \times 10^{-3}$	$0.86 \pm 3.3 \times 10^{-3}$	*	$0.87 \pm 3.3 \times 10^{-3}$	$0.86 \pm 3.1 \times 10^{-3}$	
3	$0.81 \pm 3.9 \times 10^{-3}$	$0.84 \pm 3.5 \times 10^{-3}$	*	$0.85 \pm 3.5 \times 10^{-3}$	$0.84 \pm 3.4 \times 10^{-3}$	

decision boundaries between complexity measures reveals a difference in the complexity distribution from one flight variable to another. Using k-means clustering with altitude sample entropy and permutation entropy, we were able to characterize the climb, cruise, and approach phases using three states. The states obtained from airspeed deviation were not able to clearly delineate the three flight phases.

RQ2: Differences in Entropic Dynamics Between Stable and Unstable Approaches
  Sample Entropy: The multiscale sample entropy results shown in Figs. 6, 8 and 10 depict a distinct pattern present in the complexity of all flight variables in both stable and unstable approaches; this pattern is a statistically significant difference in complexity at temporal scale 1 that tends to increase and diverge as the temporal scale increases. This multiscale pattern is mainly present in sample entropy with overlapping windows and, to a lesser extent, in sample entropy with non-overlapping windows. This pattern cannot be observed in permutation entropy in Figs. 7, 9 and 11 to the same extent. The upward trend and divergence in the complexity produced by sample entropy is a significant result from the multiscale analysis that reveals that the flight dynamics contain increasingly complex patterns at multiple temporal scales. Examining the overlapping time windows of glideslope in more detail, we note the statistically lower sample entropy (see Fig. 6 (left) and Table 4) observed in stable approaches across all time windows and temporal scales, compared to unstable approaches. The lower complexities for stable approaches are also present in the non-overlapping 2 minute and 4-minute windows in Fig. 6 (right). The high glideslope complexity observed during unstable approaches may be attributed to an unsteady descent profile due to turbulence or rapid corrective changes made to the pitch and engine power by the pilots and aviation systems that induce perturbations in the optimal 3 degree glideslope recommended by the FAA during runway approach.
  Analyzing the localizer deviation complexity in the overlapping time windows, we note an opposite trend to that of glideslope. Stable approaches exhibit higher complexity than unstable ones, with a similar pattern being noticeable in the non-overlapping windows, however, only for the 2-minute and 4-minute time windows. This pattern can be explained by the increasing number of corrective actions performed by the aircraft pilots to correct the aircraft's heading, which, according to our analysis, generally starts at the 4-minute mark before landing. Referencing Fig. 1 and [39], the aircraft is about 3,000 ft above and 9 nautical miles away from the runway at 4 minutes prior to successful or rejected landing. At this distance and time until touchdown, the localizer antenna at the airport provides a wider signal coverage, which

allows the pilots and the aircraft's autonomous systems to make last-minute corrections to the center-tracking of the aircraft to safely land in the center of the runway. Therefore, the dominating complexity during the last 4 minutes before landing translates to a higher complexity value for stable approaches at multiple temporal scales in the overlapping windows. This gives a high degree of importance to last-minute corrections made before the 1,000 ft altitude threshold that affect the overall stability of the aircraft during approach.

Similar to localizer deviation, airspeed deviation exhibits higher sample entropy values in stable approaches in the last 2-minute non-overlapping window before landing. This higher complexity, even if only present during the last stage of the approach phase, dominates the complexity across the majority of the temporal scales in the overlapping windows. Again, this indicates an increase in irregularity in the signal, which may be a consequence of increased corrective action to the heading of the aircraft as it lines up with the runway.

Multiscale sample entropy analysis provides a unique view into the evolution of unstable approach predictor variables in the last minutes prior to landing. We highlight the following observations from this analysis: 1) the high complexity of localizer deviation and airspeed deviation observed in the last stages of a stable approach (i.e., non-overlapping windows) place a significant influence on the extended temporal scales analysis (i.e., overlapping windows), causing stable approaches to report a higher complexity than unstable approaches; 2) the exception to this observation is glideslope, where a consistent trend of lower complexity in stable approaches was present that indicated that the fluctuations in the glideslope, even as far 6-minutes prior to landing, can lead to unstable approaches.

Permutation Entropy: The permutation entropy results summarized in Figs. 7, 9 and 11 and Tables 1 to 4 provide less discernible patterns in the multiscale analysis. The upwards trend in complexity as the temporal scale increases observed in sample entropy is replaced by a maximum complexity value at temporal scale 3 for glideslope and localizer non-overlapping windows. The lack of a clear-cut trend at temporal scales less than 4 for overlapping windows, due to several crossing between the unstable and stable approach curves (see glideslope and localizer deviation in Figs. 7 and 9) suggest the need to analyze the signals at higher scales. Larger temporal scales pose a challenge when studying flight variables over the short non-overlapping windows of 2 minutes, because there are not enough samples to extend the analysis to more than 3 temporal scales. This may be a limitation of data from FDRs difficult to overcome, as they are designed to sample hundreds of flight variables, but typically in the frequency range of 1-10 Hz [40].

We note that not all variables exhibit the lack of discernible patterns in the multiscale analysis results, as evidenced by the airspeed deviation results in Fig. 11. In both the overlapping and non-overlapping windows, airspeed deviation exhibits a downward trend, with a clear separation between the stable and unstable curves at time windows of 6 minutes and onward. Similar to the sample entropy results, the stable approach curves for airspeed deviation have statistically significant higher complexity than unstable approaches. We attribute the large separation between the curves at time windows closer to landing to an increase in corrective actions taken by the pilots and the aircraft to maintain the reference airspeed. Minimal deviation from the target airspeed becomes more critical closer to landing as this affects the descent profile.

Takeaways: The increasing and diverging complexity at larger temporal scales is evident in the overlapping windows closer to landing for sample entropy. The complexity during these windows can be attributed to the multitude of corrective actions performed by the pilots and aviation systems in the aircraft to maintain a safe flight profile for landing, which increases the overall complexity of the time series data and is visible at multiple temporal scales. However, not all complexity is linked to unstable approaches. This is especially the case in the results for localizer and airspeed deviation, where stable approaches tended to have higher complexity than unstable approaches at time windows closer. More importantly, observations from the multiscale analysis suggest that the complexity of signal can be potentially used as a predictor of unstable approaches at time instances of 2-6 minutes before landing. These crucial minutes prior to touchdown can be used to predict the outcome of a safe landing and provide an alert for the pilots to continue the landing approach or reject the landing and perform a go-around.

V. Conclusion

The characterization and identification of complex state changes in the flight dynamics of aircraft is a challenging problem in the field of risk and anomaly detection. Our analysis of flight variables, especially those linked to unstable approaches, using entropic methods sought to provide an interpretable method for understanding the behavior and evolution of these variables. By looking at the complexity of a flight variable, rather than attempting to discern the convoluted inner workings of advanced machine learning models, we can directly link complexity to real-world actions exhibited by pilots and aviation systems. Using complexity measurements and classical statistics, we were able to characterize the climb, cruise, and approach phases using altitude measurements and two distinct entropy measures.

Moreover, multiscale entropy analysis allowed us to observe the evolution of unstable approach predictor variables as the aircraft neared landing. The results indicated statistically significant differences in the complexity distributions of the predictor variables during a stable approach and an unstable approach. This foundational analysis using entropic methods to detect the presence of anomalies has the potential to bring more interpretable and generalizable methods for anomaly and risk prediction to the field of aviation. This will continue driving down the rate of accidents and incidents in aviation. Future work will address the use of probabilistic sensor fusion frameworks that can take advantage of the entropy distributions obtained in this study. With sensor fusion, we will be able to detect and quantify the risk linked to a potential anomaly in order to provide alerts to pilots ahead of time.

Appendix

The tables below provide additional multiscale entropy results to accompany the Results and Discussion sections.

Table 4 Glideslope deviation (GLS) multiscale entropy statistics (mean ± std. error) for overlapping time windows before landing (*: $p < 0.01$, **: $p < 0.05$).

	Sample Entropy					
	Time Window (Minutes Before Landing to Landing)					
	2 min			**4 min**		
Scale	Stable	Unstable	Significance	Stable	Unstable	Significance
1	$0.15 \pm 1.8 \times 10^{-3}$	$0.26 \pm 2.7 \times 10^{-3}$	*	$0.16 \pm 2.0 \times 10^{-3}$	$0.28 \pm 2.5 \times 10^{-3}$	*
2	$0.27 \pm 3.6 \times 10^{-3}$	$0.52 \pm 5.6 \times 10^{-3}$	*	$0.31 \pm 3.9 \times 10^{-3}$	$0.51 \pm 4.7 \times 10^{-3}$	*
3	$0.27 \pm 4.1 \times 10^{-3}$	$0.54 \pm 7.0 \times 10^{-3}$	*	$0.29 \pm 4.1 \times 10^{-3}$	$0.52 \pm 5.7 \times 10^{-3}$	*
4	—	—	—	$0.36 \pm 5.1 \times 10^{-3}$	$0.60 \pm 6.5 \times 10^{-3}$	*
5	—	—	—	$0.44 \pm 6.8 \times 10^{-3}$	$0.71 \pm 8.3 \times 10^{-3}$	*
6	—	—	—	$0.51 \pm 7.6 \times 10^{-3}$	$0.79 \pm 8.9 \times 10^{-3}$	*
	6 min			**8 min**		
Scale	Stable	Unstable	Significance	Stable	Unstable	Significance
1	$0.20 \pm 2.0 \times 10^{-3}$	$0.29 \pm 2.6 \times 10^{-3}$	*	$0.22 \pm 2.1 \times 10^{-3}$	$0.28 \pm 2.7 \times 10^{-3}$	*
2	$0.37 \pm 3.8 \times 10^{-3}$	$0.51 \pm 4.7 \times 10^{-3}$	*	$0.39 \pm 3.8 \times 10^{-3}$	$0.48 \pm 4.8 \times 10^{-3}$	*
3	$0.34 \pm 4.1 \times 10^{-3}$	$0.52 \pm 5.4 \times 10^{-3}$	*	$0.37 \pm 4.0 \times 10^{-3}$	$0.49 \pm 5.5 \times 10^{-3}$	*
4	$0.40 \pm 4.8 \times 10^{-3}$	$0.58 \pm 6.2 \times 10^{-3}$	*	$0.42 \pm 4.7 \times 10^{-3}$	$0.54 \pm 6.3 \times 10^{-3}$	*
5	$0.47 \pm 6.2 \times 10^{-3}$	$0.68 \pm 7.9 \times 10^{-3}$	*	$0.48 \pm 6.0 \times 10^{-3}$	$0.63 \pm 8.0 \times 10^{-3}$	*
6	$0.53 \pm 7.0 \times 10^{-3}$	$0.75 \pm 8.4 \times 10^{-3}$	*	$0.54 \pm 6.6 \times 10^{-3}$	$0.69 \pm 8.6 \times 10^{-3}$	*
7	$0.60 \pm 7.5 \times 10^{-3}$	$0.80 \pm 9.6 \times 10^{-3}$	*	$0.55 \pm 7.0 \times 10^{-3}$	$0.71 \pm 9.5 \times 10^{-3}$	*
8	$0.54 \pm 7.5 \times 10^{-3}$	$0.79 \pm 10 \times 10^{-3}$	*	$0.54 \pm 7.2 \times 10^{-3}$	$0.72 \pm 9.9 \times 10^{-3}$	*
9	$0.55 \pm 7.9 \times 10^{-3}$	$0.83 \pm 11 \times 10^{-3}$	*	$0.59 \pm 7.7 \times 10^{-3}$	$0.76 \pm 11 \times 10^{-3}$	*
10	—	—	—	$0.59 \pm 8.1 \times 10^{-3}$	$0.78 \pm 11 \times 10^{-3}$	*
11	—	—	—	$0.63 \pm 8.5 \times 10^{-3}$	$0.81 \pm 12 \times 10^{-3}$	*
12	—	—	—	$0.61 \pm 8.8 \times 10^{-3}$	$0.81 \pm 12 \times 10^{-3}$	*

	Permutation Entropy					
	Time Window (Minutes Before Landing to Landing)					
	2 min			4 min		
Scale	Stable	Unstable	Significance	Stable	Unstable	Significance
1	$0.78 \pm 4.1 \times 10^{-3}$	$0.89 \pm 1.6 \times 10^{-3}$	*	$0.81 \pm 4.2 \times 10^{-3}$	$0.91 \pm 1.7 \times 10^{-3}$	*
2	$0.90 \pm 4.4 \times 10^{-3}$	$0.85 \pm 2.7 \times 10^{-3}$	*	$0.89 \pm 4.3 \times 10^{-3}$	$0.91 \pm 2.2 \times 10^{-3}$	*
3	$0.93 \pm 4.5 \times 10^{-3}$	$0.83 \pm 3.0 \times 10^{-3}$	*	$0.91 \pm 4.4 \times 10^{-3}$	$0.88 \pm 2.3 \times 10^{-3}$	*
4	—	—	—	$0.89 \pm 4.5 \times 10^{-3}$	$0.87 \pm 2.8 \times 10^{-3}$	*
5	—	—	—	$0.86 \pm 4.2 \times 10^{-3}$	$0.81 \pm 2.5 \times 10^{-3}$	*
6	—	—	—	$0.84 \pm 4.1 \times 10^{-3}$	$0.78 \pm 2.5 \times 10^{-3}$	*
	6 min			8 min		
Scale	Stable	Unstable	Significance	Stable	Unstable	Significance
1	$0.84 \pm 4.3 \times 10^{-3}$	$0.90 \pm 2.2 \times 10^{-3}$	*	$0.85 \pm 4.3 \times 10^{-3}$	$0.88 \pm 2.7 \times 10^{-3}$	*
2	$0.89 \pm 4.3 \times 10^{-3}$	$0.93 \pm 2.4 \times 10^{-3}$	*	$0.90 \pm 4.3 \times 10^{-3}$	$0.94 \pm 2.6 \times 10^{-3}$	*
3	$0.89 \pm 4.3 \times 10^{-3}$	$0.92 \pm 2.4 \times 10^{-3}$		$0.91 \pm 4.2 \times 10^{-3}$	$0.94 \pm 2.5 \times 10^{-3}$	*
4	$0.88 \pm 4.2 \times 10^{-3}$	$0.91 \pm 2.8 \times 10^{-3}$	*	$0.89 \pm 4.2 \times 10^{-3}$	$0.95 \pm 2.9 \times 10^{-3}$	*
5	$0.84 \pm 3.9 \times 10^{-3}$	$0.85 \pm 2.5 \times 10^{-3}$		$0.85 \pm 3.8 \times 10^{-3}$	$0.89 \pm 2.5 \times 10^{-3}$	*
6	$0.81 \pm 3.8 \times 10^{-3}$	$0.82 \pm 2.5 \times 10^{-3}$		$0.82 \pm 3.6 \times 10^{-3}$	$0.86 \pm 2.5 \times 10^{-3}$	*
7	$0.79 \pm 3.6 \times 10^{-3}$	$0.79 \pm 2.5 \times 10^{-3}$		$0.80 \pm 3.5 \times 10^{-3}$	$0.84 \pm 2.5 \times 10^{-3}$	*
8	$0.78 \pm 3.5 \times 10^{-3}$	$0.79 \pm 2.5 \times 10^{-3}$		$0.80 \pm 3.4 \times 10^{-3}$	$0.84 \pm 2.6 \times 10^{-3}$	*
9	$0.75 \pm 3.3 \times 10^{-3}$	$0.76 \pm 2.5 \times 10^{-3}$		$0.76 \pm 3.2 \times 10^{-3}$	$0.80 \pm 2.5 \times 10^{-3}$	*
10	—	—	—	$0.74 \pm 3.1 \times 10^{-3}$	$0.79 \pm 2.6 \times 10^{-3}$	*
11	—	—	—	$0.73 \pm 3.1 \times 10^{-3}$	$0.78 \pm 2.6 \times 10^{-3}$	*
12	—	—	—	$0.74 \pm 3.1 \times 10^{-3}$	$0.79 \pm 2.6 \times 10^{-3}$	*

Acknowledgments

References

[1] Federal Aviation Administration (FAA), "Advisory Circular 120-71B – Standard Operating Procedures and Pilot Monitoring Duties for Flight Deck Crewmembers," , 2017. URL `https://www.faa.gov/documentLibrary/media/Advisory_Circular/AC_120-71B.pdf`.

[2] National Transportation Safety Board, "Aviation Accident Database & Synopses," , 2022. URL `https://www.ntsb.gov/Pages/AviationQuery.aspx`.

[3] Federal Aviation Administration (FAA), "Aviation Safety Strategic Plan FY20-FY24," , 2019. URL `https://www.faa.gov/about/office_org/headquarters_offices/avs/media/avs_strategy_508_final.pdf`.

[4] Ellis, K., Krois, P., Koelling, J., Prinzel, L., Davies, M., and Mah, R., "A Concept of Operations (ConOps) and Design Considerations for an In-time Aviation Safety Management System (IASMS) for Advanced Air Mobility (AAM)," *Proc. AIAA SciTech Forum*, 2021.

[5] International Civil Aviation Organization, "Future of Aviation," , 2019. URL `https://www.icao.int/Meetings/FutureOfAviation/Pages/default.aspx`.

[6] Hatfield, M., Cahill, C., Webley, P., Garron, J., and Beltran, R., "Integration of Unmanned Aircraft Systems into the National Airspace System-Efforts by the University of Alaska to Support the FAA/NASA UAS Traffic Management Program," *Remote Sensing*, Vol. 12, No. 19, 2020, p. 3112.

[7] U.S. Department of Transportation, Bureau of Transportation Statistics, "Transportation Statistics Annual Report 2020," , 2020. URL `https://rosap.ntl.bts.gov/view/dot/53936`.

[8] Federal Aviation Administration (FAA), "Next Generation Air Transportation System (NextGen)," , 2011. URL `https://www.faa.gov/nextgen/`.

[9] Ellis, K., Koelling, J., Davies, M., and Krois, P., "In-time System-wide Safety Assurance (ISSA) Concept of Operations and Design Considerations for Urban Air Mobility (UAM)," 2020, p. 70.

[10] Gorinevsky, D., Matthews, B., and Martin, R., "Aircraft anomaly detection using performance models trained on fleet data," *Intelligent Data Understanding (CIDU)*, 2012, pp. 17–23.

[11] Chen, D., Wang, X., and Zhao, J., "Aircraft Maintenance Decision System Based on Real-time Condition Monitoring," *Procedia Engineering*, Vol. 29, 2012, pp. 765–769. https://doi.org/10.1016/j.proeng.2012.01.038.

[12] Morris, T., and Gao, W., "Industrial Control System Cyber Attacks," 2013.

[13] *Statistical Anomaly Detection with Univariate and Multivariate Data*, John Wiley & Sons, Ltd, 2008, Chap. 14, pp. 275–289. https://doi.org/10.1002/9780470023273.ch14, URL https://onlinelibrary.wiley.com/doi/abs/10.1002/9780470023273.ch14.

[14] Yaacoub, J.-P., Noura, H., Salman, O., and Chehab, A., "Security analysis of drones systems: Attacks, limitations, and recommendations," *Internet of Things*, Vol. 11, 2020, p. 100218.

[15] Liu, L., Liu, D., Zhang, Y., and Peng, Y., "Effective Sensor Selection and Data Anomaly Detection for Condition Monitoring of Aircraft Engines," *Sensors (Basel, Switzerland)*, Vol. 16, No. 5, 2016, p. 623.

[16] Liu, L., Wang, S., Liu, D., Zhang, Y., and Peng, Y., "Entropy-based sensor selection for condition monitoring and prognostics of aircraft engine," *Microelectronics Reliability*, Vol. 55, No. 9, 2015, pp. 2092 – 2096. Proceedings of the 26th European Symposium on Reliability of Electron Devices, Failure Physics and Analysis.

[17] Xiao Hu, Hai Qiu, and Naresh Iyer, "Multivariate change detection for time series data in aircraft engine fault diagnostics," 2007, pp. 2484–2489.

[18] Li, L., "Anomaly Detection in Airline Routine Operations using Flight Data Recoder Data," Ph.D. thesis, MIT International Center for Air Transportation, 6 2013.

[19] Guangzhi Qu, Hariri, S., and Yousif, M., "Multivariate statistical analysis for network attacks detection," *The 3rd ACS/IEEE International Conference onComputer Systems and Applications, 2005.*, 2005, pp. 9–.

[20] Nanduri, A., and Sherry, L., "Anomaly detection in aircraft data using Recurrent Neural Networks (RNN)," *2016 Integrated Communications Navigation and Surveillance (ICNS)*, 2016, pp. 5C2–1–5C2–8.

[21] Das, S., Matthews, B. L., Srivastava, A. N., and Oza, N. C., "Multiple kernel learning for heterogeneous anomaly detection: algorithm and aviation safety case studys," *International conference on Knowledge discovery and data mining*, Vol. 103, 2010, pp. 47–56.

[22] Janakiraman, V. M., "Explaining Aviation Safety Incidents Using Deep Temporal Multiple Instance Learning," *International Conference on Knowledge Discovery and Data Mining*, Vol. 103, 2018, pp. 47–56.

[23] Janakiraman, V. M., "Explaining Aviation Safety Incidents Using Deep Learned Precursors," *Engineering, Computer Science, Mathematics*, 2017.

[24] Aminikhanghahi, S., and Cook, D. J., "A survey of methods for time series change point detection," *Knowledge and Information Systems*, Vol. 51, No. 2, 2017, pp. 339–367.

[25] Yan, R., Liu, Y., and Gao, R., "Permutation entropy: A nonlinear statistical measure for status characterization of rotary machines," *Mechanical Systems and Signal Processing*, Vol. 29, 2012, p. 474–484. https://doi.org/10.1016/j.ymssp.2011.11.022.

[26] Bandt, C., and Pompe, B., "Permutation Entropy: A Natural Complexity Measure for Time Series," *Phys. Rev. Lett.*, Vol. 88, 2002, p. 174102. https://doi.org/10.1103/PhysRevLett.88.174102, URL https://link.aps.org/doi/10.1103/PhysRevLett.88.174102.

[27] Shannon, C. E., "A mathematical theory of communication." *Bell Syst. Tech. J.*, Vol. 27, No. 3, 1948, pp. 379–423. URL http://dblp.uni-trier.de/db/journals/bstj/bstj27.html#Shannon48.

[28] He, S., Sun, K., and Wang, H., "Multivariate permutation entropy and its application for complexity analysis of chaotic systems," *Physica A: Statistical Mechanics and its Applications*, Vol. 461, 2016, pp. 812 – 823.

[29] Federal Aviation Administration (FAA), "Advisory Circular 91-17A – Mitigating the Risks of a Runway Overrun Upon Landing," , 2018. URL https://www.faa.gov/documentLibrary/media/Advisory_Circular/AC_91-79A_Chg_2.pdf.

[30] International Air Transport Association (IATA), "Unstable Approaches: Risk Mitigation Policies, Procedures and Best Practices," , 2017. URL https://www.iata.org/contentassets/7a5cd514de9c4c63ba0a7ac21547477a/iata-guidance-unstable-approaches.pdf.

[31] Flight Safety Foundation, "Reducing the Risk of Runway Excursions: Report of the Runway Safety Initiative," , 2017. URL https://flightsafety.org/files/RERR/fsf-runway-excursions-report.pdf.

[32] NASA, "DASHlink – Sample Flight Data," , 2012. URL https://c3.ndc.nasa.gov/dashlink/projects/85/.

[33] Odisho, E. V., and Truong, D., "Applying Machine Learning to Enhance Runway Safety Through Runway Excursion Risk Mitigation," *Proc. Integrated Communications Navigation and Surveillance Conference (ICNS)*, 2021, pp. 1–10. https://doi.org/10.1109/ICNS52807.2021.9441554.

[34] Flight Safety Foundation, "FSF ALAR Briefing Note 7.1 — Stabilized Approach," , 2000. URL https://flightsafety.org/wp-content/uploads/2016/09/alar_bn7-1stablizedappr.pdf.

[35] Zanin, M., Zunino, L., Rosso, O. A., and Papo, D., "Permutation Entropy and Its Main Biomedical and Econophysics Applications: A Review," *Entropy*, Vol. 14, No. 8, 2012, pp. 1553–1577.

[36] He, S., Sun, K., and Wang, H., "Multivariate permutation entropy and its application for complexity analysis of chaotic systems," *Physica A: Statistical Mechanics and its Applications*, Vol. 461, 2016, pp. 812–823. https://doi.org/https://doi.org/10.1016/j.physa.2016.06.012, URL https://www.sciencedirect.com/science/article/pii/S0378437116302801.

[37] Delgado-Bonal, A., and Marshak, A., "Approximate entropy and sample entropy: A comprehensive tutorial," *Entropy*, Vol. 21, No. 6, 2019, p. 541.

[38] Napoli, N. J., Mixco, A. R., Wooten, S. V., Jacopetti, M., and Signorile, J. F., "Combinational spectral band activation complexity: Uncovering hidden neuromuscular firing dynamics in EMG," *Biomedical Signal Processing and Control*, Vol. 70, 2021, p. 102891.

[39] Federal Aviation Administration (FAA), "Safety Briefing: Stabilized Approach and Landing," , 2018. URL https://www.faa.gov/news/safety_briefing/2018/media/se_topic_18-09.pdf.

[40] Federal Aviation Administration (FAA), "A Study of Sampling Rate Requirements for Load Parameter Statistics," , 2005. URL http://www.tc.faa.gov/its/worldpac/techrpt/ar05-19.pdf.